JOURNAL OF GEOPHYSICAL RESEARCH, VOL. 112, A05212, doi:10.1029/2005JA011565, 2007

Pitch angle distribution analysis of radiation belt electrons based on Combined Release and Radiation Effects Satellite Medium Electrons A data

J. L. Gannon,[1] X. Li,[1] and D. Heynderickx[2]

Received 13 December 2005; revised 7 November 2006; accepted 8 January 2007; published 22 May 2007.

[1] Using data from the Medium Electrons A instrument on the Combined Release and Radiation Effects Satellite (CRRES), a survey of pitch angle distributions (PADs) of energetic electrons is performed. The distributions are classified into three categories: 90°-peaked, flattop, and butterfly. The categorizations are examined as a function of L-shell and orbit number and at electron energies of 153, 510, and 976 keV. The 90°-peaked distributions dominate at the lowest energy channel, and butterfly distributions are more prevalent at higher L values. The PADs on the dayside are predominately 90°-peaked distributions, while butterfly distributions become more common on the nightside at higher L-shells. Fitting the PADs to a $\sin^n \alpha$ form, where α is the local pitch angle, a profile of the parameter n versus L-shell is produced for local times corresponding to postnoon and midnight sectors for the 510-keV channel. We then compare the 510-keV data during times of moderate disturbance to the less disturbed case and the average case, and show an increase in butterfly distributions, which occurs at $L > 6$ for the nightside case and $3.5 < L < 5.5$ for the dayside case. Comparing the profiles for $n > 1$ before and after the great storm on 24 March 1991, we find that there are significant differences before and after this event, the latter orbits being during a time of higher observed geomagnetic activity. Considering only those PADs with a calculated $n > 1$, the variation of the 90°-peaked distributions versus L-shell and orbit shows increased steepness at lower L-shell. For the lowest energy channel, the low L-shell variation of the steepness of the distributions visually correlates with the average 2-day minimum plasmapause location calculated from a model based on the D_{st} index over the same time period. For the 510-keV electrons, a correlation can be seen with the development of flattop distributions inside of the calculated minimum plasmapause location.

Citation: Gannon, J. L., X. Li, and D. Heynderickx (2007), Pitch angle distribution analysis of radiation belt electrons based on Combined Release and Radiation Effects Satellite Medium Electrons A data, *J. Geophys. Res.*, *112*, A05212, doi:10.1029/2005JA011565.

1. Introduction

[2] Electrons in the Earth's magnetosphere are subject to many influences, such as changes in magnetic configuration and various energization and loss processes, which are reflected in observable variations on different spatial and temporal scales. These variations depend on a number of different factors such as particle energy, spatial location, and magnetic activity. Figure 1 shows the spin-averaged flux measurements of electrons observed by the Medium Electrons A (MEA) instrument aboard Combined Release and Radiation Effects Satellite (CRRES) for the mission lifetime, versus L-shell and time (orbit number). The variations of electron fluxes at a particular location are indicative of energization, transport, and loss processes. Analyses can be performed to determine the nature of the process as regards phase space density conservation, providing additional clues in identifying the particular process. Another important characteristic of electrons are their pitch angle distributions. Particles of different pitch angles react to different influences in different ways. Changes in the pitch angle distribution (PADs) at a particular location can give us important clues to the factors producing electron flux variations.

[3] PADs of outer radiation belt electrons may be generally classified into three categories, 90°-peaked, flattop, and butterfly, which are associated with different physical processes. The most common type of distribution in the inner magnetosphere for electrons of energies of hundreds of kiloelectron volts is characterized by a maximum flux around 90° [*West et al.*, 1973]. We call this a 90°-peaked distribution. Note that this is a broader definition than is usually made and includes rounded distributions, normal (Gaussian) distributions, and the rarer strongly anisotropic

[1] Laboratory for Atmospheric and Space Physics, Boulder, Colorado, USA.
[2] Institute for Space Aeronomy, Brussels, Belgium.

0148-0227/07/2005JA011565$09.00

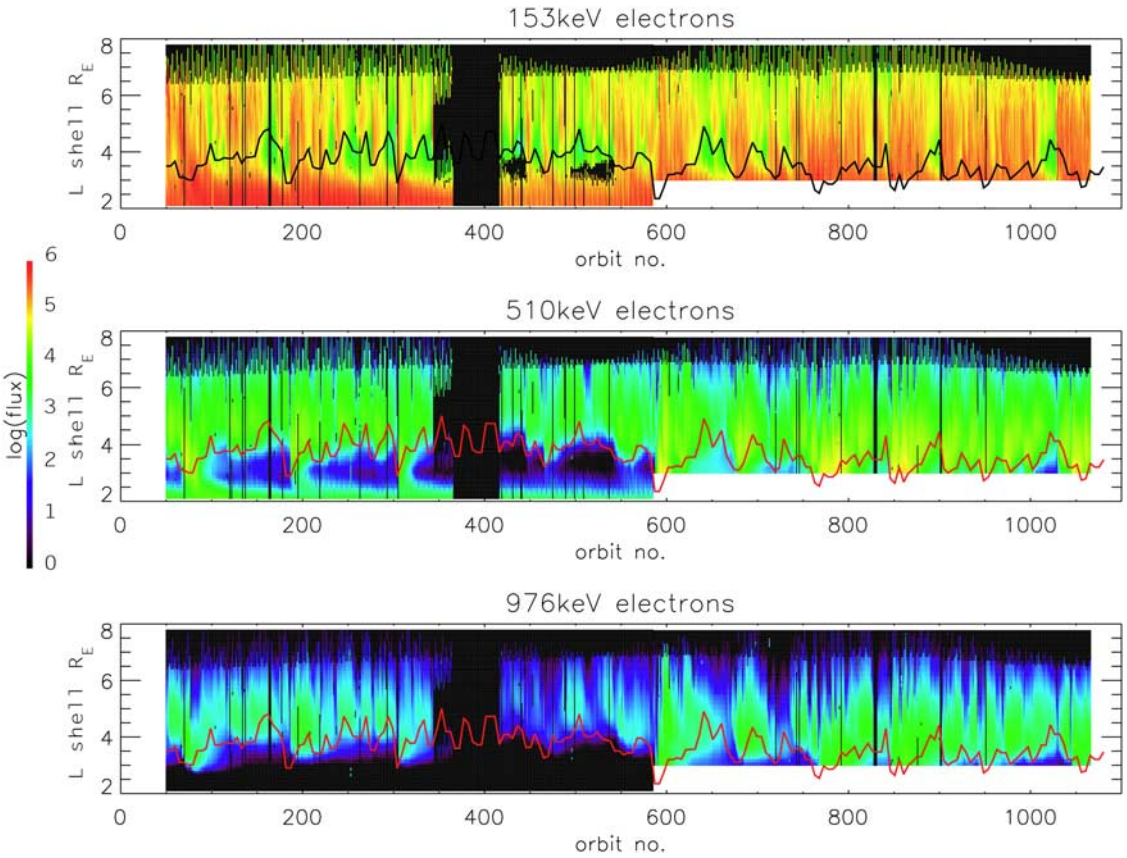

Figure 1. Spin-averaged flux measurements throughout the entire CRRES mission, binned by L-shell (y axis) and orbit number (x axis), for the incoming pass of each orbit. The color scale specifies the log of the measured flux. The panels, from top to bottom, refer to differential channel central energies of 153, 510, and 976 keV. The black and red overlay curves show the 2-day minimum average plasmapause location from the model of *O'Brien and Moldwin* [2003], based on D_{st}. Orbit 6-1067 refers to calendar dates 27 July 1990 to 12 October 1991.

distributions typically called pancake distributions (named because of their appearance in velocity space). The 90°-peaked distributions are often fit to a form $\sin^n \alpha$, such that the parameter n describes the steepness of the flux peak around 90°. Inward radial diffusion can cause a flux increase around 90°, or, equivalently, an increase in the numerical value of the parameter n is needed to fit the distribution. This increased peaking is due to conservation of the first adiabatic invariant and the relative abundance of lower-energy electrons. As a particle moves inward while conserving its first and second adiabatic invariants, its momentum perpendicular to the field line is increased more than its momentum parallel to the field line [*Schulz and Lanzerotti*, 1974]. An equatorially mirroring particle has no parallel momentum component, so an increase in perpendicular momentum corresponds directly to an increase in total kinetic energy. This, as well as the relative abundance of the lower-energy particles, results in a greater increase in flux around 90° through inward radial diffusion. The 90°-peaked distributions are also observed in lower-energy populations and have been associated with whistler mode waves and electron cyclotron harmonic waves acting upon electrons of energies ranging from 100 eV to 30 keV by *Meredith et al.* [1999]. *Meredith et al.* [2000] studied low-energy particles (100 eV < E < 30 keV) measured by the low-energy plasma analyzer (LEPA) on CRRES and calculated a "pancake index" based on the ratio of the flux at 90° and the flux at 70° in each distribution. They showed that the observed formation of 90°-peaked distributions on a 2-hour timescale is consistent with whistler-wave-associated pitch angle diffusion outside of L = 6. Inside L = 6, they suggest that electron cyclotron harmonic waves near the plasmapause contribute to the peaking of the distributions that is too strong to be explained by whistler waves alone. Although these results are not directly comparable to our work because of the energy dependence of the processes, they show that overlapping processes contribute to the complexity of pitch angle distribution changes.

[4] The butterfly distribution has a minimum around 90°. These distributions can be indicative of magnetopause shadowing, drift shell splitting, or wave-particle interactions. Magnetopause shadowing occurs because of the asymmetry of the magnetosphere: compressed dayside and stretched nightside. For a group of particles beginning on the same magnetic field line on the nightside, equatorially mirroring particles drift out farther on the dayside than particles with other pitch angles [*Roederer*, 1970]. Particles drifting farther out are more likely to be lost through the magnetopause, appearing as a loss around 90° when the particles return to the nightside. Without being lost through

the magnetopause, a butterfly distribution of energetic electrons can still be formed because of the magnetic field asymmetry. This process, called drift-shell splitting, can produce butterfly distributions on the nightside because of distortions from a dipolar configuration, as explained by *Selesnick and Blake* [2002]. The drift shell of a particle is determined by its mirror point on the same field line. In a field with a local-time asymmetry, if a particle is fully adiabatic, the radial distance of the equatorial crossing point of that drift shell will be different at different local times for particles of different pitch angles. Particles of different pitch angle have different L-shells at the same radial location, which is referred to as drift-shell splitting. In order to produce a butterfly distribution from this effect, there must also be a gradient in the radial profile of particle flux [*Roederer*, 1970]. If there is decreasing flux with radial distance, and equatorially mirroring particles are at a higher L-shell than other pitch angle, there will be an observed depression in the PAD around 90° [see, e.g., *Selesnick and Blake*, 2002]. Wave-particle interactions have also been theorized to be able to produce butterfly distributions [*Horne et al.*, 2003a]. If a localized process energizes 90° pitch angle particles at an off-equatorial location, when the distribution is mapped back to the equator, where the pitch angles of these particles are not 90°, the PAD can appear as a butterfly distribution.

[5] The flattop distribution is characterized by approximately equal flux at most pitch angles. It can sometimes be seen as a transitional stage between a 90°-peaked and butterfly distribution. In addition, flattop distributions have been linked to wave-particle interactions during storm recovery phase at higher L-shells by *Horne et al.* [2003a].

[6] Previous studies have examined in detail changes in PAD for particular time periods. *Horne et al.* [2003a] studied a single storm from the MEA data (orbits 185–192) during October 1990 in order to determine the contribution of different acceleration processes. They observed butterfly distributions at the onset of the main phase, consistent with drift shell splitting. *Brautigam and Albert* [2000] discussed the consistency of 90°-peaked distributions at $L > 6$ at low energies, but near $L = 4$, the case is not as clear. The observed flattop distributions could be the result of inward radial diffusion from a butterfly distribution at an outer L-shell, but they state that the observed flux enhancement for higher-energy electrons (with the first adiabatic invariant > 700 MeV/G) is too large to be explained by radial diffusion alone. Both works note studies citing the energy dependence of the pitch angle distributions as a reason that radial diffusion cannot be working alone.

[7] In a recent work by *Fritz et al.* [2003], butterfly PADs at higher L-shells are found to be associated with magnetopause shadowing, based on electron (22.5 keV to 1.2 MeV) and proton (24 keV to 2 MeV) observations from ISEE-1. This work also shows an energy dependence in the radial position of the transition from lower L-shell 90°-peaked distributions to higher L-shell butterfly distributions in near-equatorial observations. In addition, *Selesnick and Blake* [2002] performed a survey of equatorial outer radiation belt pitch angle distributions measured by Polar, observing anisotropies consistent with the effects of drift shell splitting.

[8] Using similar classification techniques as *Meredith et al.* [2000], we examine electron PADs at energies from the CRRES MEA, similar in energy range to the *Fritz et al.* [2003] work, but also studying PAD variations at L-shells lower than those associated with magnetopause shadowing.

2. Spacecraft and Data

2.1. CRRES Medium Electrons A

[9] The CRRES satellite operated from July 1990 through October 1991 in a geostationary transfer orbit (altitude: 350 km × 5.2 R_e), with an 18° inclination and a 10-hour orbital period. Its relatively low inclination positions it well to observe PADs directly, as few particles will mirror nearer to the equator, not being observed. The MEA instrument is a 180° magnetic drift spectrometer that measures electron counts from 153 keV to 1.582 MeV in 17 differential energy channels [*Vampola et al.*, 1992]. The satellite spins at a rate of 2.2 rpm and samples every half of a second, yielding an approximately 6° scan for every measurement interval. Usually, geometric information is used to determine pitch angle information from a detector, and more complicated means are used to determine the energy of the incident particles. However, the MEA uses geometric information to accurately determine the energy with little contamination and, from its single aperture, uses a mathematical description and extensive prelaunch testing to associate a pitch angle with a measured sample. Before launch, the instrument response was modeled based on aperture width and energy-dependent geometric factors, and was calibrated and tested based on known particle distribution inputs. The real incident particle distribution could then be known based on detector output from operation in space. From comparison to prelaunch calibrations, pitch angle information is assigned to data. The range of pitch angles sampled is a function of the angle between the spin axis of the instrument and the magnetic field line [*Vampola*, 1998]. This method of assigning pitch angle distributions does not give a unique solution, but a probable one, and is the best solution available for the detector configuration.

2.2. Calibrations and Corrections

[10] Several corrections to the MEA data set are needed to adjust for instrument thresholds and proton contamination. For the MEA, when the count rate exceeds approximately 35,000 counts per second, an instrument threshold is reached, resulting in the detector counting down for subsequent fluxes. This foldover, which usually occurs in lower-energy channels, was corrected at the time of the mission from knowledge of instrument response and prelaunch calibrations. The count level never reached twice the instrument threshold, so that a single foldover correction was sufficient in all cases. The correction was done using information from higher-energy (lower flux) channels.

[11] In addition, it is necessary to correct for background proton contamination. The MEA instrument included a proton channel which is scaled and subtracted from the recorded electron counts. Different energy-dependent scaling factors should be used in the inner and outer zones (defined in this study as inside and outside $L = 2.5$), but as we are only concerned with the outer zone, only those coefficients are used [*Vampola et al.*, 1992]. In order to convert count reported by the detector into differential flux, we used the

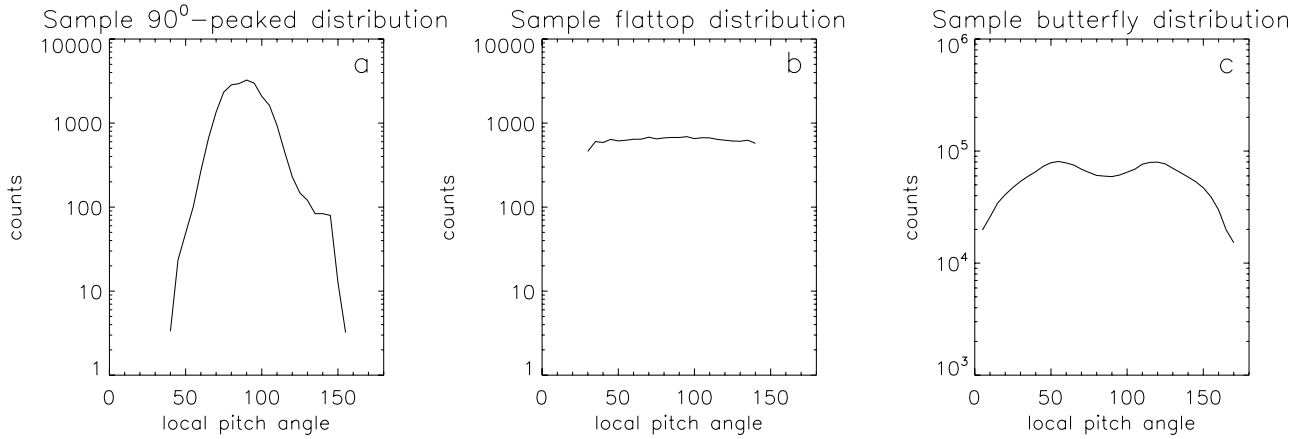

Figure 2. Examples taken from the 510-keV data of the three distribution classifications used in this study: (a) 90°-peaked, (b) flattop, (c) butterfly.

following form based on the half-second sampling rate and central energy of each differential channel:

$$j(i) = \frac{1}{\sigma_E}(\text{counts}(i) - \text{background} \times \text{coefficient}(i))$$

The symbol σ_E represents the energy-dependent geometric factors (GEFs) used for each channel [*Vampola et al.*, 1992]. The index i refers to each of the 17 energy channels. As well as flux and pitch angle information, each measurement is accompanied by magnetic local time, altitude, and L-shell information.

[12] In order to organize the data, we averaged the measurements into bins of 0.1 L, 5° in pitch angle, and inbound orbit number (in order to average measurements in nearby spatial locations). We then have pitch angle distributions versus L for every other half-orbit. We classify these distributions into one of the three standard types based on the ratio of flux at 90° to the average of the fluxes at 45° and 135°. A perfect flattop distribution would have a ratio of 1 (flux at 90° equals flux at 45° and 135°). We define a flattop to include those distributions where the flux at 90° is within 10% of the average at 45° and 135°. The 90°-peaked and butterfly distributions are defined as those where the ratio is greater than 1.1 and less than 0.9, respectively. Figure 2 shows examples of each of the classifications.

3. Survey

[13] Figure 3 shows the summary of distribution classifications versus L-shell and orbit number for inbound orbits for three different energies. Red represents 90°-peaked, blue are butterfly, and green are flattop distributions. The PADs' highly variable nature is immediately evident. Changes can occur on a timescale of one orbit (10 hours) or several days. There is an apparent dependence on orbit, which will later be shown to be a local-time dependence, and L. Data below $L = 3.0$ after 24 March 1991 are not shown because of high-energy electron contamination from the new radiation belt electrons appearing during that day [*Vampola et al.*, 1992; *Blake et al.*, 1992; *Li et al.*, 1993; *Gannon et al.*, 2005].

[14] Changes in the steepness of 90°-peaked distributions can also reflect the action of physical processes (for example, inward radial diffusion leading to steeper 90°-peaked distributions). In Figure 4, the color scale represents the n values calculated from the fit to $\sin^n(\alpha)$ based on the following approximation, from the work of *Vampola* [1998]:

$$n\left(\log\left(\frac{I_{90}}{I_{45-135}}\right) + 0.004105\right)/0.14303$$

where I_{90} is the flux at 90° and I_{45-135} is the average of the flux at 45° and 135°.

[15] In the figure, the brighter areas indicate very sharply peaked distributions, and black corresponds to flatter distributions ($n = 1$). Those distributions with $n < 1$ are not included and are shown as data gaps, the white areas. The 90°-peaked distributions are typically steeper at lower L, but the timescale of variation is different at different L-shells. One factor in the steepness of 90°-peaked distributions is the relative location to the magnetic equator. *Meredith et al.* [1999] suggested that, based on the work of *Parks* [1991], 90°-peaked distributions are more sharply peaked when measured at the magnetic equator. This could also be a contributing factor to the observed lower n values at higher L-shells.

[16] The overlay curve in Figures 3 and 4 show the modeled 2-day minimum plasmapause location versus CRRES orbit [*O'Brien and Moldwin*, 2003]. This model is not local-time-dependent but shows the average L-shell for the plasmapause at a given time as a function of the D_{st} index, a major index measuring the strength of the ring current and used to determine the phase and strength of a magnetic storm. The position of the plasmapause is dependent on magnetic activity. In times of a higher cross-tail electric field, the $E \times B$ drift of plasmaspheric particles is increased and the boundary of the plasmasphere is pushed inward. A correlation with the pitch angles of particles inside the plasmapause can be seen in the two higher-energy classification plots (Figure 3). Several examples of the appearance of flattop distributions (for example, near orbit 650 in the 510-keV channel) seem to correlate with, and remain inside of the boundary of, the plasmaspheric region. The appearance of flattop distributions corresponds to a decrease in the n parameter, or less peaking around 90°. In

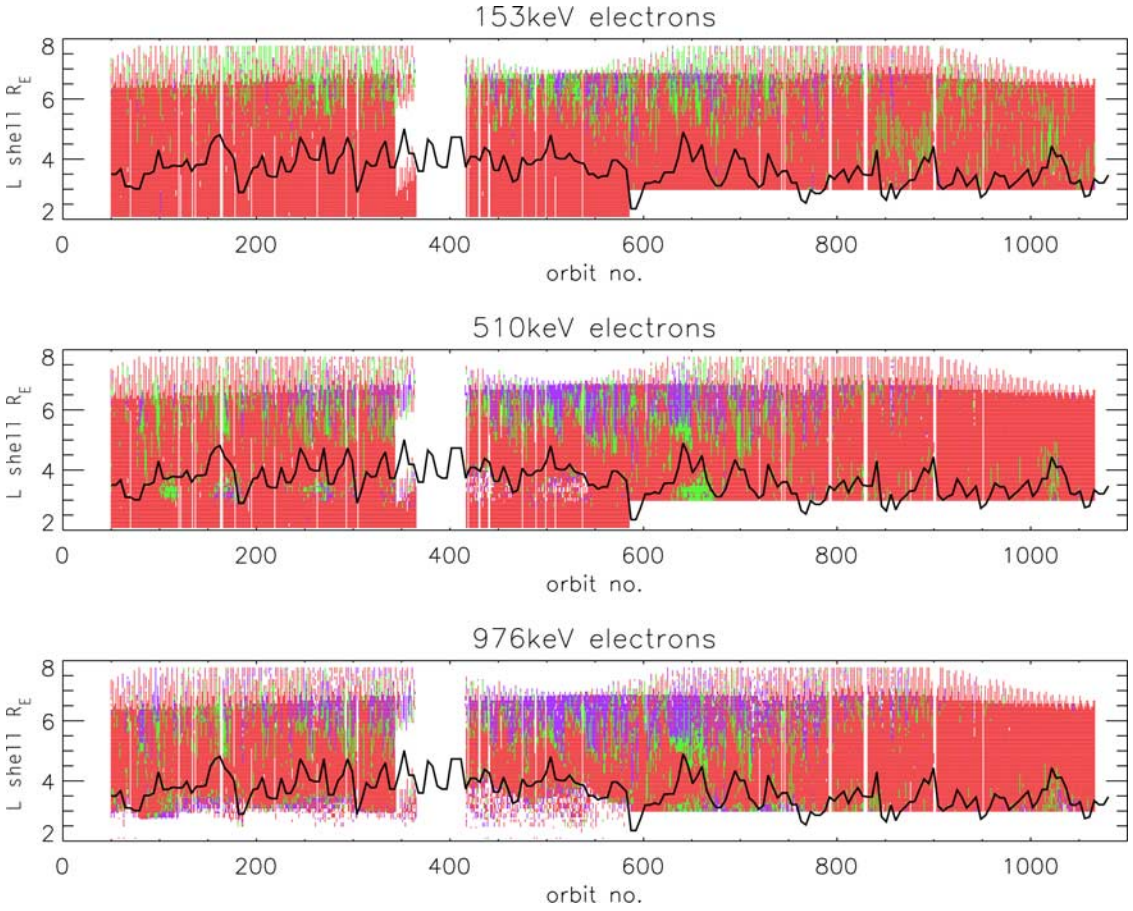

Figure 3. Survey plots of the classifications of pitch angle distribution type seen throughout the entire CRRES mission, binned by L-shell (*y* axis) and orbit number (*x* axis) for the incoming pass of each orbit. The color scale denotes the classifications as follows: red, 90°-peaked; blue, butterfly; and green, flattop. The panels, from top to bottom, refer to differential channel central energies of 153, 510, and 976 keV. The black curve shows the 2-day minimum average plasmapause location from the model of *O'Brien and Moldwin* [2003], based on D_{st}.

contrast, in the low-energy channel (153 keV), a correlation with the plasmapause location is more easily seen with the steepness of 90°-peaked distributions (Figure 4). Inside the plasmapause, the more peaked distributions appear to correlate with, and remain inside of, the minimum plasmapause boundary. These observations appear to be consistent with pitch angle scattering with plasmaspheric hiss. This whistler mode emission tends to be confined to high-density regions inside the plasmasphere and in detached plasma regions at high *L*. Plasmaspheric hiss can persist during relatively quiet conditions, but the emission intensifies during storms and substorms [*Smith et al.*, 1974; *Thorne et al.*, 1974, 1977; *Horne et al.*, 2003a; *Meredith et al.*, 2004]. *Lyons et al.* [1972] computed equatorial pitch angle distributions resulting from resonant interactions with plasmaspheric hiss for decaying slot region electrons at $L = 2$, 3, and 4 for various energies. At low energies ($E < 200$ keV), strong 90°-peaked distributions are predicted for $L < 4$. At higher energies ($E = 500$ keV), flat-topped distributions are predicted at $L = 4$, but strong 90°-peaked distributions are predicted at $L = 2$ and $L = 3$. At even higher energies ($E > 1$ MeV), the predicted distributions are flat-topped for $L > 3$. Very recently, *Li et al.* [2006] identified and discussed the correlation between the inner edge of the outer radiation belt electrons and the innermost plasmapause location (Lpp). They outlined mechanisms by which the plasmapause may play a role in modifying the acceleration and loss processes of the electrons as follows: (1) the pitch angle scattering of the electrons by very low frequency (VLF) and electromagnetic ion cyclotron (EMIC) waves that is probably responsible for the precipitation which occurs mostly near the Lpp; (2) the plasmasphere may modify the characteristics of the ultralow frequency (ULF) waves that diffuse particles radially inward and to higher energies; (3) the VLF chorus acceleration mechanism may produce a flux peak just outside the plasmasphere because it is strongest just beyond the plasmapause. However, they also noted that it is still not clear which of the likely explanations contributes more to the correlation.

3.1. Local Time

[17] Separating the data by magnetic local time gives us a clearer picture of the dependence of a pitch angle distribution on position, and the distortion of the magnetic field. The top panels of Figures 5 and 6 show measurements from the 510-keV channel in two different local-time ranges, corresponding to midnight (22:30–01:30 MLT) and post-

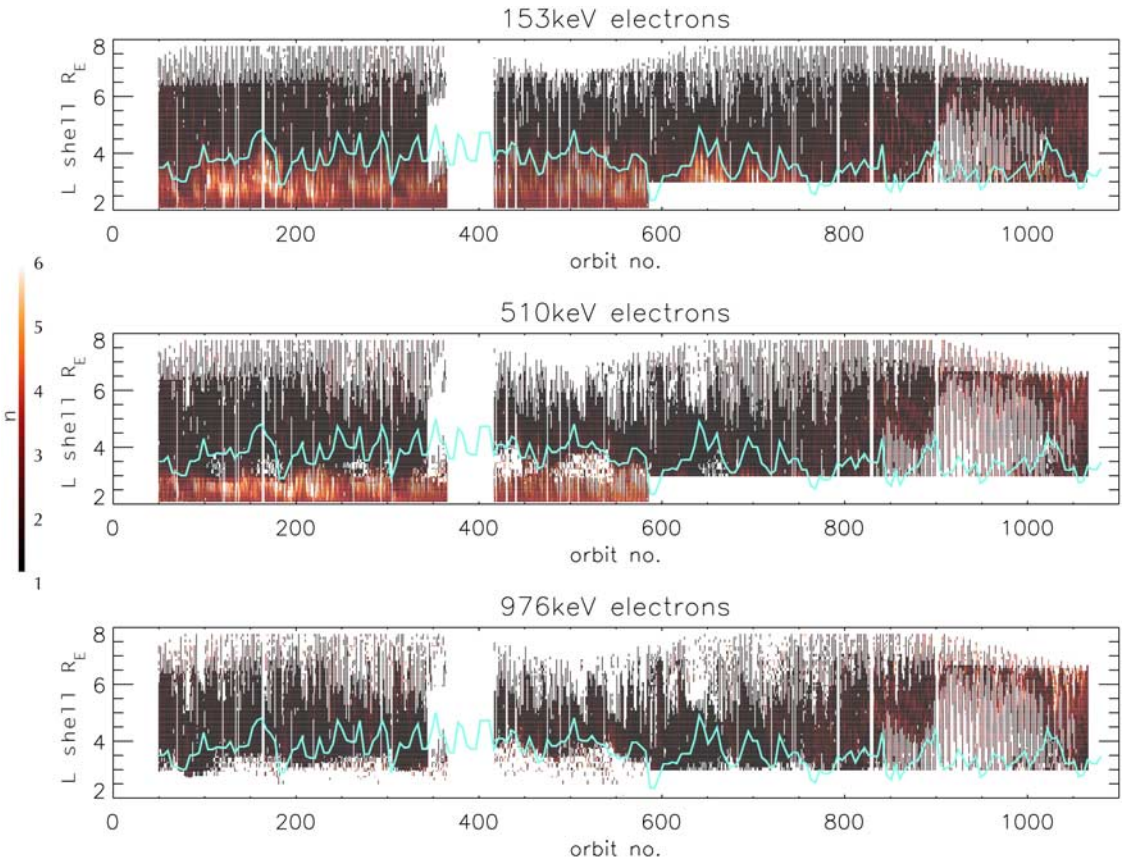

Figure 4. Considering only distributions with an approximated n greater than 1, the steepness of the distribution is shown by the color scale, versus L-shell (y axis) and orbit number (x axis) for incoming orbital passes. The panels, from top to bottom, correspond to differential channel central energies of 153, 510, and 976 keV, respectively. The blue curve shows the 2-day minimum average plasmapause location from the model of *O'Brien and Moldwin* [2003], based on D_{st}.

noon (13:00–16:00). The left-hand panel in each figure shows the percentages of each of the three types of PAD versus L. The afternoon distributions are almost completely dominated by 90°-peaked distributions. Around midnight, where the field lines are more stretched, butterfly distributions begin to strongly contribute beyond $L = 5$. These trends are reflected in the right-hand panel of each figure, which show the fit to a $\sin^n \alpha$ form versus L, as described earlier. Our findings are consistent with the work by *Vampola* [1998], where it was shown that the steepness of PADs is highly dependent on local time, though only those distributions with $n > 1$ were considered. We show here that including butterfly distributions makes the local-time dependence even more obvious.

[18] We then compare the average case to times when D_{st} is between 0 and −25 nT (quiet conditions) and also to times when D_{st} is between −25 and −50 nT (moderately disturbed conditions), with a local-time constraint. The middle and bottom panels of Figures 5 and 6 show the quiet time and moderately disturbed case, respectively, for the two time periods discussed previously, midnight, and afternoon. Even with a slight enhancement of disturbance, the amount of butterfly distributions is increased. On the nightside, the increase in butterfly distributions occurs at $L > 5$. On the dayside, though not as much, an increase occurs at a lower L ($3.5 < L < 5.5$). One possibility is that this is a result of magnetopause shadowing which radially diffuses inward and then drifts through all local times.

3.2. Magnetic Activity

[19] As shown earlier, magnetic activity has a significant impact on the PADs. Orbit 587 marks the onset of the great storm of 24 March 1991. The period following this event can be generally characterized as having a higher geomagnetic activity level than the period before, based on the D_{st} index. Figure 7a shows the average calculated n value versus L-shell in the 510-keV channel for the entire CRRES mission, which is similar to the work of *Vampola* [1998], although, in that work, the distributions were first binned by local time and then averaged. Here we average the distributions without regard to local time. Figures 7b and 7c show the subset of orbits before and after orbit 587. A significant difference in PADs is seen at all L-shells. After the storm, there is an increase in the parameter n at higher L-shells: The distributions are more peaked around 90°. The cause of this difference could be a coincidental result of the geomagnetic activity level (or the solar activity) or as a direct result of the storm on the particle populations in the radiation belts. The effect of the 24 March 1991 storm may have been greater on equatorially mirroring particles, resulting in an increase in the parameter n. However, the

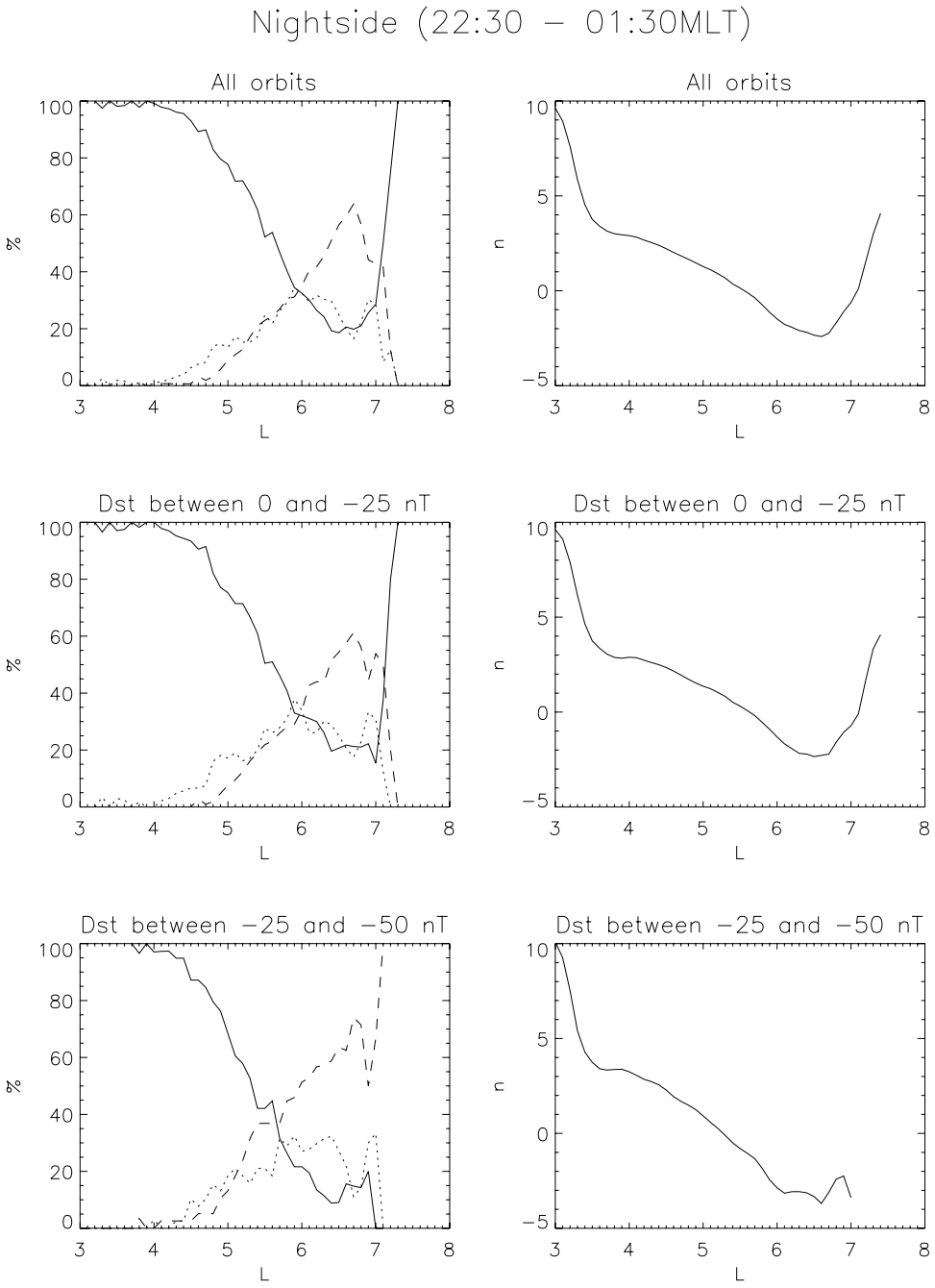

Figure 5. For electrons in the 510-keV channel, the percentage of each classification type (left column) and the calculated n value (right column) are shown versus L-shell for nightside (22:30–1:30) orbits. The subsets of orbits shown are average case (all orbits, top plots), only those orbits where D_{st} is between 0 and −25 nT (middle plots), and only those orbits where D_{st} is between −25 and −50 nT (bottom plots). In the three left panels, the solid line shows the percentage of pancake distributions, the dashed line shows butterfly, and the dotted line shows flattop distributions.

increase in n is more dramatically seen at higher L-shells after the event, while the flux increases after the storm were observed most dramatically near $L = 2.5$.

3.3. PAD Persistence

[20] The persistence of a given pitch angle distribution is difficult to calculate definitively because of the dynamic nature of the magnetosphere. Distributions are constantly changing because of energization and loss processes. Statistically, we can look at the persistence of the three classifications of PAD over the CRRES mission. Because we know that the distribution form is highly dependent on local time, we separate the samples that we previously categorized versus orbit into 2-hour local-time sections. Then, for each L, we count the number of orbits of persistence of each classification type. Figure 8 shows three local-time examples

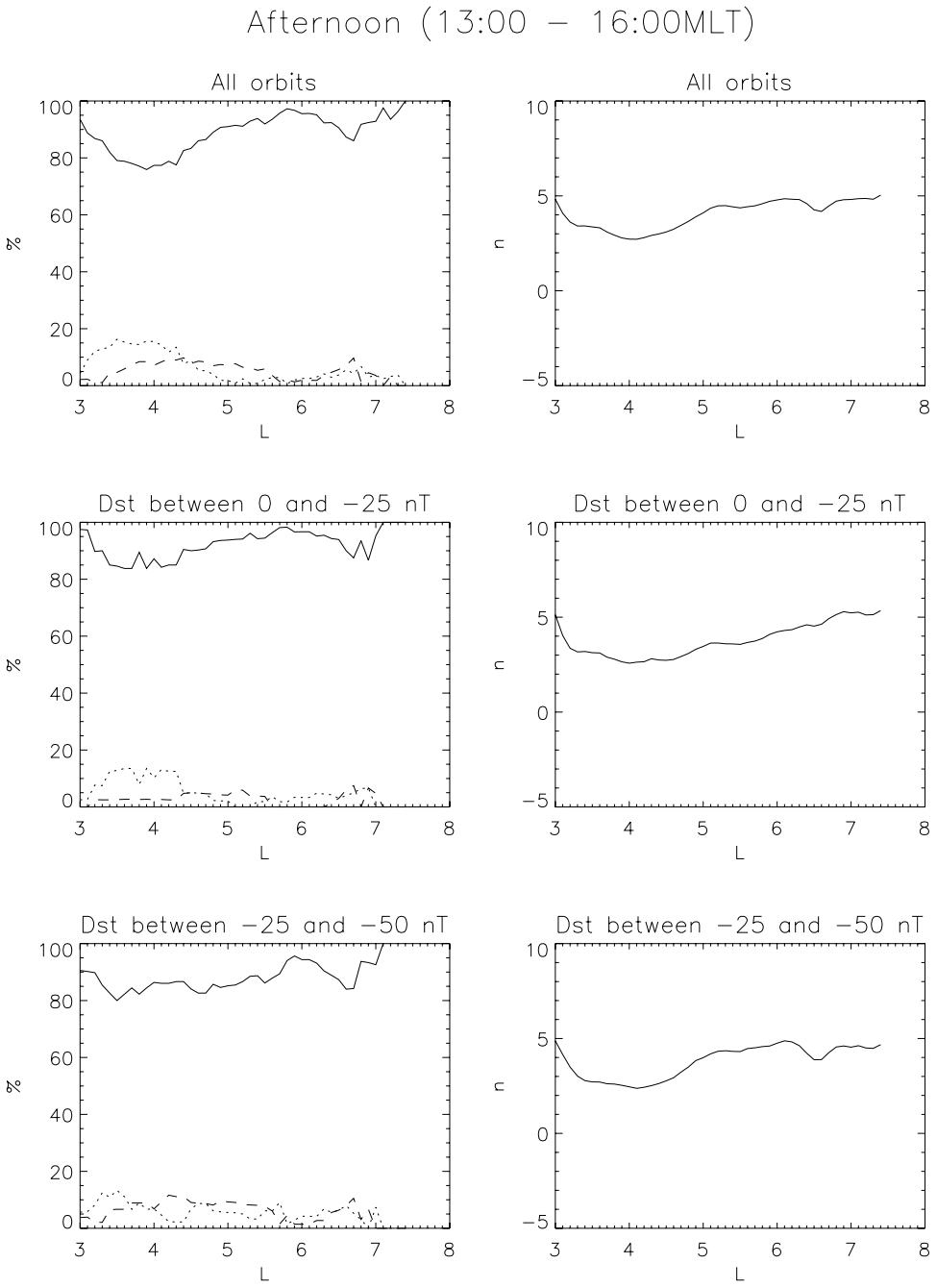

Figure 6. For electrons in the 510-keV channel, the percentage of each classification type (left column) and the calculated n value (right column) are shown versus L-shell for nightside (13:00–16:00) orbits. The subsets of orbits shown are average case (all orbits, top plots), only those orbits where D_{st} is between 0 and −25 nT (middle plots), and only those orbits where D_{st} is between −25 and −50 nT (bottom plots). In the three left panels, the solid line shows the percentage of pancake distributions, the dashed line shows butterfly, and the dotted line shows flattop distributions.

of the average PAD duration versus L-shell. It can first be seen that 90°-peaked distributions are the longest-lasting type, although this may be due to the fact that it is the broadest definition and the most prevalent type. The survey does not take into account how the 90°-peaked distributions change in steepness over successive orbits. Butterfly and flattop distributions are rather short-lived, lasting one or two orbits before another type is observed. The persistence of the butterfly distribution has an understandable relation to L-shell and local time. Closer to midnight, where these distributions are more likely to be observed at larger L-shells, the persistence increases.

4. Discussion

[21] Different types of PADs of electrons are associated with different physical processes. Inward radial diffusion causes a flux increase around 90° faster than other pitch

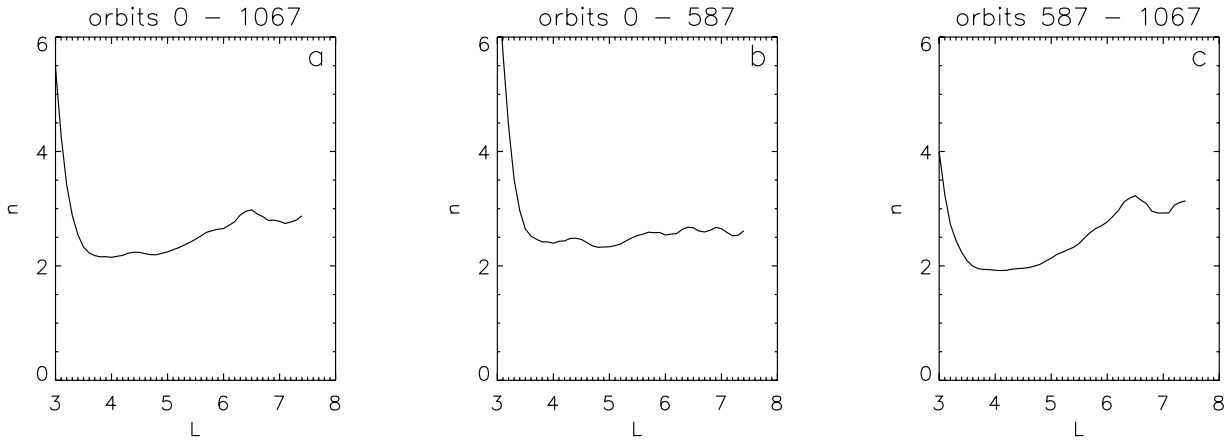

Figure 7. Comparison of average calculated n value versus L, for (a) all orbits, and (b) before and (c) after the great storm of 24 March 1991.

angles. This creates an increased peaking for distributions starting as 90°-peaked distributions or can change an apparent butterfly distribution at higher L to a flattop and eventually to a 90°-peaked distribution at a lower L. Radial diffusion is typically more effective on lower-energy particles. A particle is energized by field fluctuations that have frequencies comparable to that particle's drift period. Lower-energy particles interact with lower frequency fluctuations, which typically have more available power [*Schulz and Lanzerotti*, 1974; *Li*, 2006]. Comparing the three energy examples described earlier, there are greater numbers of 90°-peaked distributions at lower energies, especially at higher L-shells. Although the drift-shell splitting process itself is not energy-dependent, the effects are more likely to be observed at higher energies because of their stronger radial gradient in fluxes. A component that is consistent with inward radial diffusion is the evolution of butterfly distributions at higher L-shells and flattop and 90°-peaked distributions at lower L-shell. This is discussed by *Horne et al.* [2003a] as a possible explanation of how radial diffusion may be acting, even with the observance of flattop distributions near $L = 4$. There are several examples of butterfly distributions evolving to lower L-shells and becoming flattop over successive orbits (see, for example, Figure 3, orbits 625–650 between $L = 4.0$ and $L = 6.0$ for the 510-keV energy). In this theory, the butterfly distributions at the higher L-shells undergo radial diffusion, resulting in flattop distributions at lower L-shells. Over successive orbits, the radial range of the flattop distributions should increase as the butterfly distributions diffuse from higher L. The 90°-peaked distributions at lower L are affected by the inward diffusion of flattop distributions. However, flattop distributions are also observed at lower L, which is not explained by the above argument. In order to definitively associate the examples observed with radial diffusion, a study at constant first invariant would be required. Similar to the works by *Meredith et al.* [2000] and *Horne et al.* [2003a, 2003b] described previously, we also observe variations in the types of distribution with energy which are obvious from the survey plots alone.

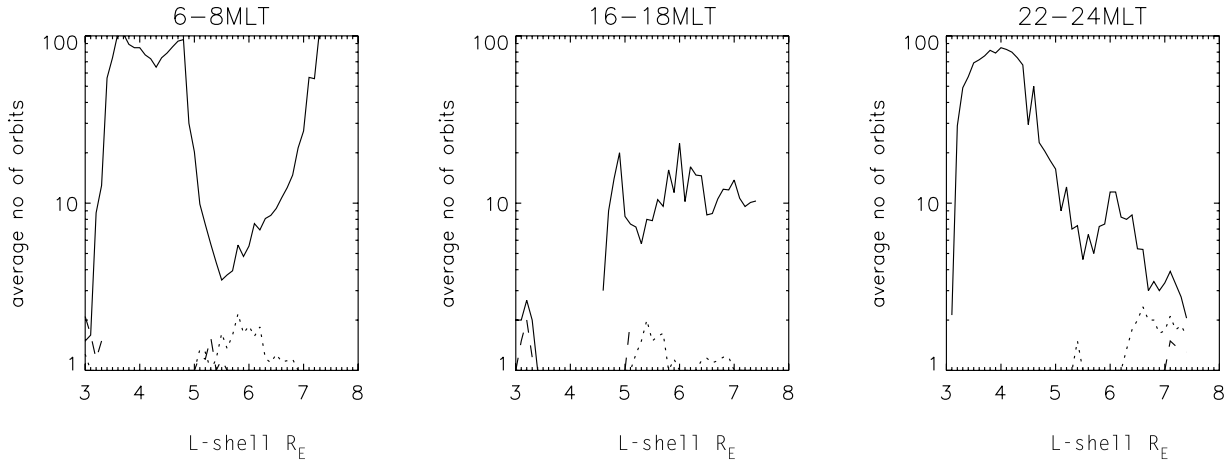

Figure 8. Average distribution lifetimes over the entire CRRES mission versus L, for incoming orbital passes in the 510-keV channel for three different local times. The solid line shows that 90°-peaked distributions have the longest average lifetime, but their dependence on L-shell varies with local time. Butterfly distributions, marked by the dotted line, typically last from 1 to 2 orbits, depending on L-shell, and flattop distributions, marked by the dashed line, are the most quickly varying.

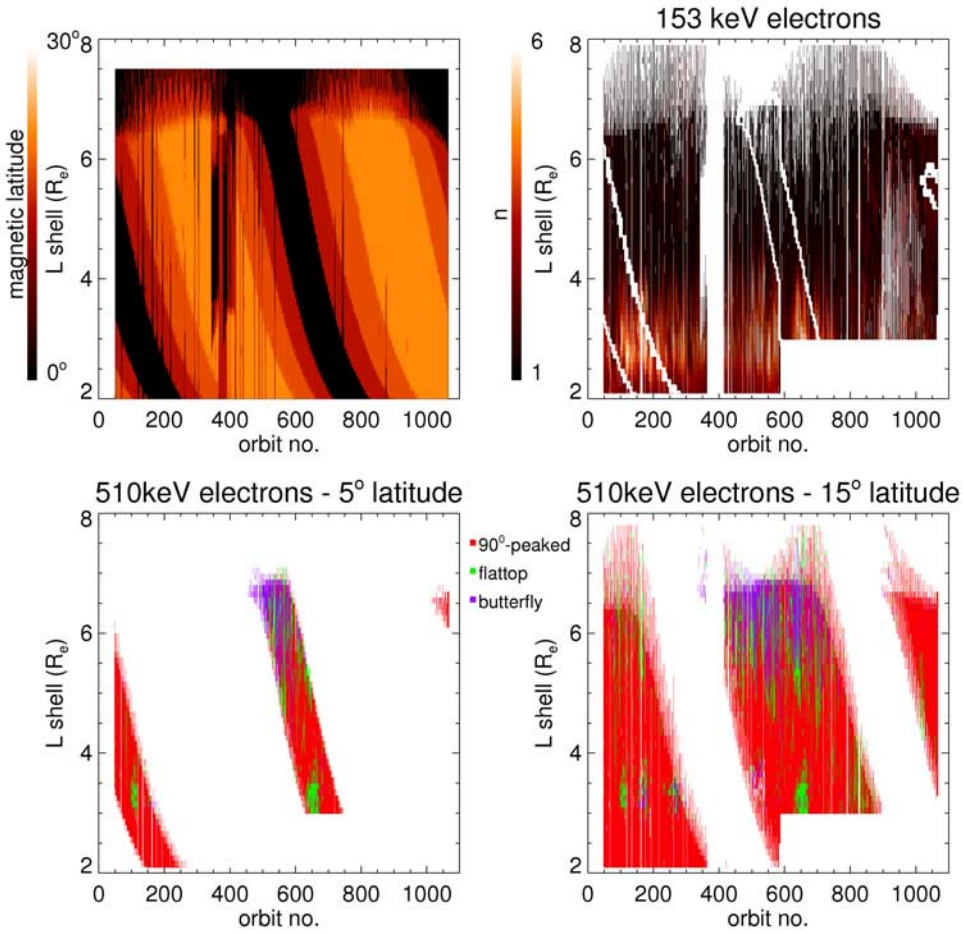

Figure 9. Magnetic latitudes crossed by CRRES during its mission. The color scale shows the absolute value of the magnetic latitude. (b) Calculated n value of the observed pancake distributions in the 153-keV channel. The contours are placed every 5° in magnetic latitude, from Figure 9a. (c) Those distribution classifications for the 510-keV channel limited to those times when CRRES was within 5° of the magnetic equator. (d) Similar to Figure 9c, limited to 15° of the magnetic equator.

[22] If a change in pitch angle distribution is due to a loss process, there should be an associated decrease in flux. Using the distributions obtained for the survey plots, in the 510-keV channel, we select distributions that begin as butterfly distributions and, in the course of one orbit, change to 90°-peaked distributions at the same local time and L-shell. The number of times this occurs when the flux is increased at all pitch angles is compared with the number of times it occurs with a decrease in flux, at a particular L-shell. At $L = 6.6$, the number of PADs associated with decreases and increases are approximately equal. During the opposite change (a 90°-peaked distribution becoming a butterfly distribution), about two thirds are associated with an increase implying that this change is more likely associated with an energization process rather than a loss process.

[23] The varying magnetic latitude of these measurements with the orbit adds another level of complexity in comparing one PAD to another. Figure 9a shows the absolute value of magnetic latitude during the CRRES mission, calculated using the Olsen-Pfitzer model. We would expect variations between local and equatorial PADs. When the measurement is made away from the equator, only a subset of particles on a field line are measured. Under a simple dipole, a magnetic latitude of 10° allows equatorial pitch angle coverage of 0°–69°. For a particle with a magnetic latitude of 20°, the range is 0°–50°. In addition, the pitch angle value assigned to a particle is different than at the equator. For example, an off-equatorial measurement of 90° implies that the particle is mirroring at the satellite location and therefore would not be measured as a 90° pitch angle particle at the equator. It would appear as, perhaps, a 60° or 120° particle. The flux associated with a particular pitch angle equatorially is therefore shifted to a different pitch angle observation locally. For flattop distributions, where the flux would be equal at all pitch angles in the ideal case, this should have little effect. For 90°-peaked and butterfly distributions, the effect is a lessening of the steepness of the difference between the flux at 90° and 45°. This is consistent with the derivation of *Meredith et al.* [1999], which predicted decreased peaking for off-equatorial pitch angle distributions. We can see this in data in Figure 9. The appearance of the 90°-peaked distributions in Figure 9b is brighter (steeper) inside contours of lower latitude (<5°). However, even with the broad range in latitudes (−30° to 30°) during the CRRES mission, there seems to be little difference in the overall classifications of PAD types observed. All three types appear during periods of both high- and low-latitude

measurement (see Figures 9c and 9d). There are more butterfly distributions seen during times of low-latitude satellite positioning; however, contributions from the strong local-time dependence at higher L-shells could be more significant.

5. Summary

[24] The many influences magnetospheric electrons are subject to can reflect themselves in different ways in variations of relative flux levels and pitch angle distribution. The different clues provided by changes in PADs and flux level can be used in combination to suggest a particular physical process. We study the variations in PAD in order to contribute to that larger goal. Pitch angle distributions are classified into three categories (90°-peaked, flattop, and butterfly). General trends observed include a greater number of 90°-peaked distributions at lower energies and on the dayside, and greater number of butterfly distributions at higher L values and on the nightside. Using an approximation of the sine function, we fit distributions to a $\sin^n \alpha$ form and produce a profile of the parameter n versus L-shell for local times corresponding to postnoon and midnight. The distributions during times of moderate disturbance (-50 nT $< D_{st} < -25$ nT) are compared to the average case and the slightly disturbed case (-25 nT $< D_{st} < 0$ nT), and show an increase in butterfly distributions occurring for both dayside and nightside cases. The increase occurs at $L > 6$ on the nightside and $3.5 < L < 5.5$ on the dayside. The calculated n value versus L-shell also shows significant variation before and after orbit 587, which corresponds to a significant change in the electron populations due to the event of 24 March 1991, but is also a dividing point between the observed low- and high-activity periods of the first and second halves of the mission, respectively. A visual correlation is seen between the 2-day average minimum plasmapause location and the steepness of 90°-peaked distributions inside that location for 153-keV electrons. A correlation is also observed between this plasmapause location and the appearance of flattop distributions for the higher-energy channels. The length of time a PAD can persist on average is L-shell-dependent. The 90°-peaked distributions persist longer than flattop or butterfly distributions, whose lifetimes are typically 1 or 2 orbits (10–20 hours). An example of a PAD evolution at higher L-shells is consistent with radial diffusion, although examples at lower L-shells and near the plasmapause boundary are inconsistent with that description.

[25] **Acknowledgments.** We are indebted to A. Vampola for providing the original CRRES/MEA data and his willingness to discuss the data analysis. We also thank both reviewers for their useful comments and T. A. Johnson for his help with figure improvements. This work was supported in part by NASA (NAG-13518) and NSF grants (ATM-0233302), and by the Center for Integrated Space Weather Modeling (CISM), which is funded by the STC Program of the National Science Foundation under Agreement ATM-0120950.

[26] Zuyin Pu thanks Nigel Meredith and another reviewer for their assistance in evaluating this paper.

References

Blake, J. B., W. A. Kolasinski, R. W. Rillius, and E. G. Mullen (1992), Injection of electrons and protons with energies of tens of MeV into L < 3 on March 24, 1991, *Geophys. Res. Lett.*, *19*, 821.

Brautigam, D. H., and J. M. Albert (2000), Radial diffusion analysis of outer radiation belt electrons during the 9 October 1990, magnetic storm, *J. Geophys. Res.*, *105*, 291.

Fritz, T. A., M. Alothman, J. Bhattacharjya, D. L. Matthews, and J. Chen (2003), Butterfly pitch angle distributions observed by ISEE-1, *Planet. Space Sci.*, *51*(3), 205–219.

Gannon, J. L., X. Li, and M. Temerin (2005), Parametric study of shock-induced transport and energization of relativistic electrons in the magnetosphere, *J. Geophys. Res.*, *110*, A12206, doi:10.1029/2004JA010679.

Horne, R. B., N. P. Meredith, R. M. Thorne, D. Heynderickx, R. H. A. Iles, and R. R. Anderson (2003a), Evolution of energetic electron pitch angle distributions during storm time electron acceleration to megaelectronvolt energies, *J. Geophys. Res.*, *108*(A1), 1016, doi:10.1029/2001JA009165.

Horne, R. B., R. M. Thorne, N. P. Meredith, and R. R. Anderson (2003b), Diffuse auroral electron scattering by electron cyclotron harmonic and whistler mode waves during an isolated substorm, *J. Geophys. Res.*, *108*(A7), 1290, doi:10.1029/2002JA009736.

Li, X., I. Roth, M. Temerin, J. Wygant, M. K. Hudson, and J. B. Blake (1993), Simulation of the prompt energization and transport of radiation belt particles during the March 24, 1991 SSC, *Geophys. Res. Lett.*, *20*, 2423.

Li, X. (2006), The role of radial transport in accelerating radiation belt electrons, AGU Monograph Series on Recurrent Magnetic Storms: Corotating Solar Wind Streams.

Li, X., D. N. Baker, T. P. O'Brien, L. Xie, and Q. G. Zong (2006), Correlation between the inner edge of outer radiation belt electrons and the innermost plasmapause location, *Geophys. Res. Lett.*, *33*, L14107, doi:10.1029/2006GL026294.

Lyons, L. R., R. M. Thorne, and C. F. Kennel (1972), Pitch angle diffusion of radiation belt electrons within the plasmasphere, *J. Geophys. Res.*, *77*, 3455.

Meredith, N. P., A. D. Johnstone, S. Szita, R. B. Horne, and R. R. Anderson (1999), "Pancake" electron distributions in the outer radiation belts, *J. Geophys. Res.*, *104*(A6), 12,431–12,444.

Meredith, N. P., R. B. Horne, A. D. Johnstone, and R. R. Anderson (2000), The temporal evolution of electron distributions and associated wave activity following substorm injections in the inner magnetosphere, *J. Geophys. Res.*, *105*(A6), 12,907–12,917.

Meredith, N. P., R. B. Horne, R. M. Thorne, D. Summers, and R. R. Anderson (2004), Substorm dependence of plasmaspheric hiss, *J. Geophys. Res.*, *109*, A06209, doi:10.1029/2004JA010387.

O'Brien, T. P., and M. B. Moldwin (2003), Empirical plasmapause models from magnetic indices, *Geophys. Res. Lett.*, *30*(4), 1152, doi:10.1029/2002GL016007.

Parks, G. K. (1991), *Physics of Space Plasmas*, Addison-Wesley, Boston, Mass.

Roederer, J. G. (1970), *Dynamics of Geomagnetically Trapped Radiation*, Springer, New York.

Schulz, M., and L. J. Lanzerotti (1974), *Particle Diffusion in the Radiation Belts*, Springer, New York.

Selesnick, R. S., and J. B. Blake (2002), Relativistic electron drift shell splitting, *J. Geophys. Res.*, *107*(A9), 1265, doi:10.1029/2001JA009179.

Smith, E. J., A. M. Frandsen, B. T. Tsurutani, R. M. Thorne, and K. W. Chan (1974), Plasmaspheric hiss intensity variations during magnetic storms, *J. Geophys. Res.*, *79*, 2507.

Thorne, R. M., E. J. Smith, K. J. Fiske, and S. R. Church (1974), Intensity variation of ELF hiss and chorus driving isolated substorms, *J. Geophys. Res.*, *1*, 193.

Thorne, R. M., S. R. Church, W. J. Malloy, and B. T. Tsurutani (1977), The local time variation of ELF emissions during periods of substorm activity, *J. Geophys. Res.*, *82*, 1585.

Vampola, A. L., J. Osborn, and B. Johnson (1992), The CRRES Magnetic Electron Spectrometer, *J. Spacecr. Rockets*, *29*, 592–594.

Vampola, A. L. (1998), Outer Zone Energetic Electron Environment Update, in *Proceedings of the Conference on the High Energy Radiation Background in Space; Snowmass, CO, USA; July 22, 1997*, volume IEEE Conference Proceedings, pp. 128–136.

West, H. I., Jr., R. M. Buck, and J. R. Walton (1973), Electron Pitch Angle Distributions throughout the Magnetosphere as Observed on Ogo 5, *J. Geophys. Res.*, *78*(7).

J. L. Gannon, Space Environment Center, NOAA, W/NP9, 325 Broadway, Boulder, CO 80305, USA. (jennifer.gannon@noaa.gov)

D. Heynderickx, Institute for Space Aeronomy, Brussels, Belgium. (d.heynderickx@oma.be)

X. Li, Laboratory for Atmospheric and Space Physics, 1234 Innovation Drive, Boulder, CO 80303, USA. (xinlin.li@lasp.colorado.edu)